



Article

Mechanical, Thermal, and Morphological Properties of Graphene Nanoplatelet-Reinforced Polypropylene Nanocomposites: Effects of Nanofiller Thickness

Harekrushna Sutar ¹, Birupakshya Mishra ¹, Pragyan Senapati ^{2,*}, Rabiranjana Murmu ¹ and Dibyani Sahu ¹

¹ Department of Chemical Engineering, Indira Gandhi Institute of Technology, Sarang 759146, India; h.k.sutar@gmail.com (H.S.); bir.mishra7@gmail.com (B.M.); rabiranjana_murmu@rediffmail.com (R.M.); sahudibyani006@gmail.com (D.S.)

² Department of Mechanical Engineering, Siksha'O'Anusandhan (Deemed to Be University), Bhubaneswar 751030, India

* Correspondence: pragyansenapati@soa.ac.in; Tel.: +91-943-958-3624

Abstract: In this work, polypropylene (PP) and graphene nanoplatelet (GNPs) composites are routed through twin screw mixing and injection moulding. Two types of GNPs with a fixed size of 25 μm with surface areas ranging from 50–80 m^2/g (H25, average thickness 15 nm) and 120–150 m^2/g (M25, average thickness 6–8 nm) were blended with PP at loading rates of 1, 2, 3, 4, and 5 weight%. Mechanical properties such as tensile, flexural, and impact strengths and Young's modulus (E) are determined. The X-ray diffraction (XRD), differential scanning calorimetry (DSC), thermogravimetric analysis (TGA), dynamic mechanical analysis (DMA), field emission scanning electron microscopy (FESEM), and polarised light microscopy (PLM) techniques are used to understand the crystallisation, thermal, dynamic mechanical, and structural behaviour of the prepared composites. The improvement of mechanical strength is observed with GNP loading for both grades. Decreasing the GNP thickness decreases the impact strength and on the other hand improves the tensile and flexural strengths and Young's modulus. Maximum tensile (≈ 33 MPa) and flexural (≈ 58.81 MPa) strength is found for the composite carrying 5 wt% M25. However, maximum impact strength (0.197 J) is found for PP-5 wt% H25. XRD analysis confirms GNPs have an induction effect on PP's β phase crystal structure. The PP-GNP composite exhibits better thermal stability based on determining the T_D (degradation temperature), T_{10} (temperature at 10% weight loss), T_{50} (temperature at 50% weight loss), and T_R (temperature at residual weight). Enhancement in melt (T_m) and crystallisation temperatures (T_c) is observed due to a heterogeneous nucleation effect. The FESEM analysis concludes that the GNP thickness has a significant effect on the degree of dispersion and agglomeration. The smaller the thickness, the better is the dispersion and the lower is the agglomeration. Overall, the use of thinner GNPs is more advantageous in improving the polymer properties.

Keywords: polypropylene; graphene; nanocomposite; mechanical; thermal; thickness effect



Citation: Sutar, H.; Mishra, B.; Senapati, P.; Murmu, R.; Sahu, D. Mechanical, Thermal, and Morphological Properties of Graphene Nanoplatelet-Reinforced Polypropylene Nanocomposites: Effects of Nanofiller Thickness. *J. Compos. Sci.* **2021**, *5*, 24. <https://doi.org/10.3390/jcs5010024>

Received: 7 December 2020

Accepted: 11 January 2021

Published: 14 January 2021

Publisher's Note: MDPI stays neutral with regard to jurisdictional claims in published maps and institutional affiliations.



Copyright: © 2021 by the authors. Licensee MDPI, Basel, Switzerland. This article is an open access article distributed under the terms and conditions of the Creative Commons Attribution (CC BY) license (<https://creativecommons.org/licenses/by/4.0/>).

1. Introduction

Graphene, a new material, has attracted considerable attention in recent scientific literature. Graphene nanoplatelets (GNPs) are graphite nano crystals in multiple layers that exist by virtue of van der Waals forces. Polymer composites with GNPs have a wide range of applications in the field of materials sciences [1–8]. Among the groups of polyolefin, polypropylene (PP) is the most acceptable commodity product [9–11]. PP is cheap, facilitates easy processing and recycling, and has good mechanical strength and physical properties [12–16]. Many researchers tried to improve its properties by reinforcing GNP as nano filler [17–19]. The scientific literature reveals GNP loading augments both mechanical and thermal behaviour. Polymer nanocomposites with graphene as a filler show improved mechanical and electrical characteristics than clays, carbon fibres and carbon

black as filling agents [20–22]. An observation shows improvement of flexural modulus up to 9 GPa for composites filled with 20 volume % GNPs [23], but the same composite loaded with conventional fillers gains flexural strength less than 7 GPa. Small-sized GNP composites perform well as far as mechanical strength is concerned but have poor electrical conductivity [24]. High dispersibility is feasible for large-sized GNPs, thereby improving in electrical property due to reduced percolation threshold, but at an equal loading rate, GNPs with higher aspect ratios accelerate percolation within the polymer chain. This is considerably important when nanoparticles of an insignificant amount are incorporated in the polymer matrix, so it is possible to use a small amount of nanofillers without causing mechanical failure. In other words, it can be said that the performance of the nanocomposites is a function of the physical properties of the GNPs. Yun-Seok Jun et al used very large-sized GNPs ($\approx 150 \mu\text{m}$) to add to the PP matrix, and the composite's thermal, mechanical, and electrical properties were studied [25]. They verified that large-sized GNPs are unsatisfactory for development of mechanical strength due to distortion at the time of melt compounding thereby reducing the aspect ratio. This further reduced the interfacial strength between the polymer matrix and filling agent. Liang et al [26] improved the tensile modulus of virgin PP (1.25 GPa) by 100% by reinforcing GNPs of size less than $10 \mu\text{m}$ and thickness smaller than 5 nm. It was reported that the GNP loading capacity declines with increasing size. Chunhui et al [27] examined the flexural strength and proved that it is inversely related to the size of GNPs. Bafana et al [28] studied the thermal behaviour of the polypropylene matrix by incorporating GNPs. They demonstrated that filling 1.5 wt% of GNP increased $T_{10\%}$ (temperature at 10% mass loss) by 29°C . Pedrazzoli et al [29] reported the presence of GNP significantly altered the crystallization behaviour of a polymer matrix. They revealed that an increase of isothermal crystallisation (at 145°C) rate up to 380% occurred with the addition of 0.01 wt% of GNPs. Their report also revealed up to 11% growth of PP's β crystals at 1 wt% loading of GNPs. However, limited studies are available that compare the effect of the sheet size and thickness of GNPs.

The above description shows the GNP-reinforced polymer matrix improves the variety of properties and is solely dependent on its physical properties, so selecting a specific sheet size and thickness is extremely important to maximise the composite performance. Small-sized GNPs are preferred for light-weight automobile parts to increase fuel efficiency [30]. GNP composites may also be useful for manufacturing packing materials for carrying chemicals and fuels. Large-sized GNPs are preferable for enhancing electrical conductivity [31–33]. Further research is still essential to understand the effect of different properties of GNPs on the performance of the polymer composites. Hence, in this paper, an attempt has been made for deep explanation of the effect of GNP sheet thickness and loading rates on various physiochemical properties of its composite with PP. The current study is carried broadly at a constant sheet size of $25 \mu\text{m}$ (diameter) with average thicknesses of 15 nm and 6–8 nm.

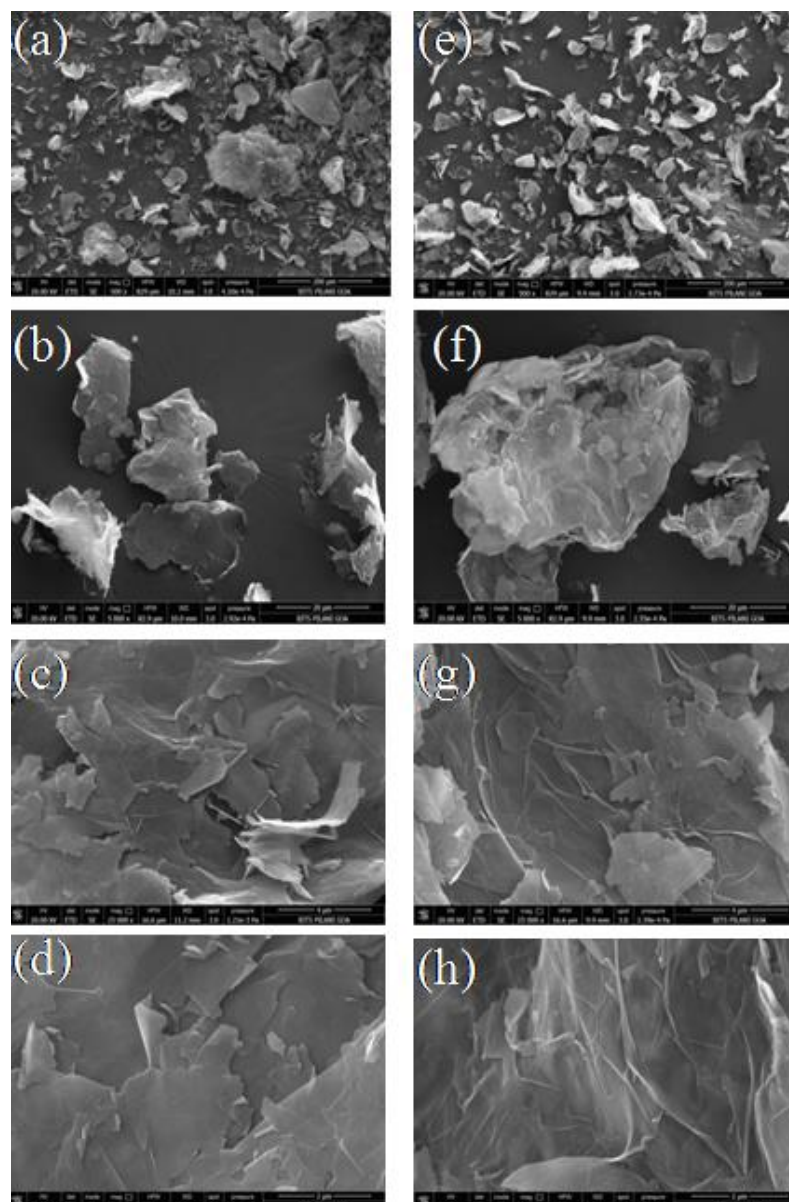
2. Materials and Preparations

2.1. Materials

PP in pellet (M110 Grade, homopolymer) form with a typical diameter of about three mm was procured from Haldia Petrochemicals private limited, Haldia, India, and used as a polymer matrix. The melt flow index of this used PP was determined as per American Society for Testing and Materials (ASTM) D1238 standard (230°C , 11 kg) and reported to be 11 g/10 min. The polymer has a density of 0.900 g/cc. Graphene nanoplatelets (GNPs) were obtained from Sigma Aldrich chemical company (XG science) St. Louis, MO, United States. Two different grades of GNPs are used for this study. The different properties of the used GNPs are mentioned in Table 1 and the reported data are from the technical data sheet of XG science. To understand the morphology of the available GNPs, the FESEM images are shown in Figure 1 at different magnifications.

Table 1. Typical properties of the procured GNPs.

Grades of GNPs.	H25	M25
Code Name	GH	GM
Diameter (size), μm	25	25
Thickness, nm	15	6–8
Surface area, m^2/g	50–80	120–150
Bulk density, g/cc	0.03–0.1	0.03–0.1
Oxygen Content, wt%	<0.5	<0.5
Residual acid content, wt%	<1	<1

**Figure 1.** Field emission scanning electron microscope (FESEM) images of GNPs for each grade: (a–d) H25 and (e–h) M25 at $500\times$ (a,e), $5000\times$ (b,f), $25,000\times$ (c,g) and $50,000\times$ (d,h) magnifications.

2.2. Preparation of Composites

The virgin polypropylene (PP) was mixed separately with each grade of GNP. Initially, both the PP and GNPs were successfully suspended using ethyl alcohol and agitated to achieve improved distribution. Both of them were dried at 60 °C overnight in a vacuum oven. The GNP powder was manually added to PP at 1, 2, 3, 4, and 5 weight %. The mixture was circulated for 5 min before melt compounding. A twin screw extruder (PTW 16, Thermo Electron Corporation, Langensfeld, Germany) was used for melt mixing. The minimum operating temperature of the extruder was 190 °C at the feeder and a maximum of 210 °C in the fourth zone. The melt and die temperatures were 220 and 200 °C, respectively. The processing was carried out at a screw speed of 30 rpm with a residence time of 80 s. The obtained composites in pelletised form were moulded in an injection moulding machine (Endura-90, Electronica plastic machines limited, Pune, India) at a barrel temperature of 180 °C to obtain the test specimens. The prepared composites and sample codes are mentioned in Table 2.

Table 2. Prepared composites and corresponding sample codes.

Filler wt%	PP wt%	Sample Code
H25/GH		
0.0	100.0	PP
1.0	99.0	PP-GH1
2.0	98.0	PP-GH2
3.0	97.0	PP-GH3
4	96.0	PP-GH4
5	95.0	PP-GH5
M25/GM		
1.0	99.0	PP-GM1
2.0	98.0	PP-GM2
3.0	97.0	PP-GM3
4	96.0	PP-GM4
5	95.0	PP-GM5

3. Material Characterisations

3.1. Mechanical Strength Measurements

Tensile specimens with a size as per ASTM D638-02a (Type I, gauge length 50 mm) were prepared. Tensile strength was determined using a universal testing machine (UTM3382, Norwood, MA, USA) at a cross head speed of 50 mm/min. Flexural samples of size 127 mm × 12.7 mm × 3.2 mm were prepared. A three-point bending method was adopted to carry out the flexural tests as per ASTM D790 standards. The speed of the flexural test was calculated following Equation (1). The flexural strength (σ_{Fmax}) in MPa is reported as per Equation (2).

$$\text{Speed} = \frac{ZL^2}{6d} \quad (1)$$

$$\sigma_{Fmax} = \frac{3PL}{2bd^2} \quad (2)$$

The operating straining rate (Z) was 0.01 mm/mm/min and support span length was 51.2 mm. The span length (L) was sixteen times the thickness (d). The strain was applied up to an extension of 10% at a speed of 1.365 mm/min. The notations P and b are the applied load and specimen width, respectively. Impact test specimens of 63.5 mm × 12.7 mm × 3.2 mm were prepared having a 45° V-notch of 25 mm depth. Tests were conducted using a charpy impact meter (IT 504 Plastic impact, Tinius Olsen, Horsham, PA, USA) following ASTM

D256-A standards. All the above tests were carried out at room temperature. Five repeated trials were carried out for each evaluation and the average value is given.

3.2. Thermal Properties

The nanocomposites' thermal behaviour was studied conducting DSC and TGA experiments. The DSC analysis was carried out using a DSC-60A plus instrument manufactured by Shimadzu in Japan. At first the samples were heated from room temperature to 300 °C at a heating rate of 10 °C/min. The earlier thermal history was erased by keeping the samples at 300 °C for five minutes. Hereafter, the samples were cooled to room temperature under a nitrogen (N₂) environment at 10 °C/min. Then, the second heating cycle followed the same conditions, and the necessary data were collected. Various thermal properties such as melting enthalpy (ΔH_m), melting (T_m), and crystallisation (T_c) temperatures and degree of crystallinity (X_c) were traced from DSC analysis. The % crystallinity of each sample was determined using Equation (3).

$$\text{Degree of Crystallinity}(X_c) = \frac{\Delta H_m}{\phi \times \Delta H_m^\circ} \quad (3)$$

where ΔH_m is the melting enthalpy, ϕ is the weight% of PP in the nanocomposite, and ΔH_m° is the enthalpy corresponding to 100% crystalline PP and is given as 209 J/g [34]. The thermal stability of the nanocomposites was analysed by conducting TGA experiments using a Shimadzu DTG-60H apparatus made in Japan. The test samples were heated in a nitrogen environment with a flow rate of 50 mL/min. About 20 mg of each sample was heated from room temperature to 600 °C at a rate of 10 °C/min to analyse their degradation behaviour.

3.3. Structural and Morphological Study

XRD analysis of the PP, GNPs, and the composites was conducted on a Rigaku Miniflex with Cobalt (Co) K α radiation at $\lambda = 1.79 \text{ \AA}$. The surface morphology of the samples was assessed with the help of a field emission scanning electron microscope (FESEM, Quanta FEG 250) at an acceleration voltage of 20 kV, and all the samples were gold sputter coated (LEICA EM ACE 200) with 3 nm thickness. A polarised light microscope (PLM, Leica, DM750P, Wetzlar, Germany) was used to identify the crystallisation morphology (spherulite structure) of the virgin PP and the prepared nanocomposites. A small piece of sample was placed on the glass slide and was heated using a hot stage to melt at 200 °C. The molten sample was converted to a thin film by sandwiching it in a micro glass slide. The molten sample was allowed to cool using a cold stage. Both heating and cooling stages were conducted at 5 °C/min. The spherulite images were captured at 130 °C at 10 \times magnification.

3.4. Dynamic Mechanical Analysis

In order to understand the viscous and elastic behaviour of the samples, DMA tests were carried out by simultaneous application of stress, frequency, and temperature. The tests were performed following ASTM D 5026 standards on a DMA Q 800, TA instruments, New Castle, DE, USA in single cantilever bending mode. The size of the specimens was 35 mm \times 12 mm \times 3 mm. The experiment was conducted at a frequency of 1 Hz under a nitrogen atmosphere from 20 °C to 160 °C at a heating rate of 10 °C/min.

4. Results and Discussion

4.1. Tensile, Flexural and Impact Strength

The effect of GNP loading on different mechanical properties was determined by performing the tests as mentioned earlier. Tensile strength, maximum tensile load, and Young's modulus (E) as a function of the GNP content are plotted in Figure 2. The data are extracted and tabulated in Table 3. It is observed that the tensile strength increased with GNP loading.

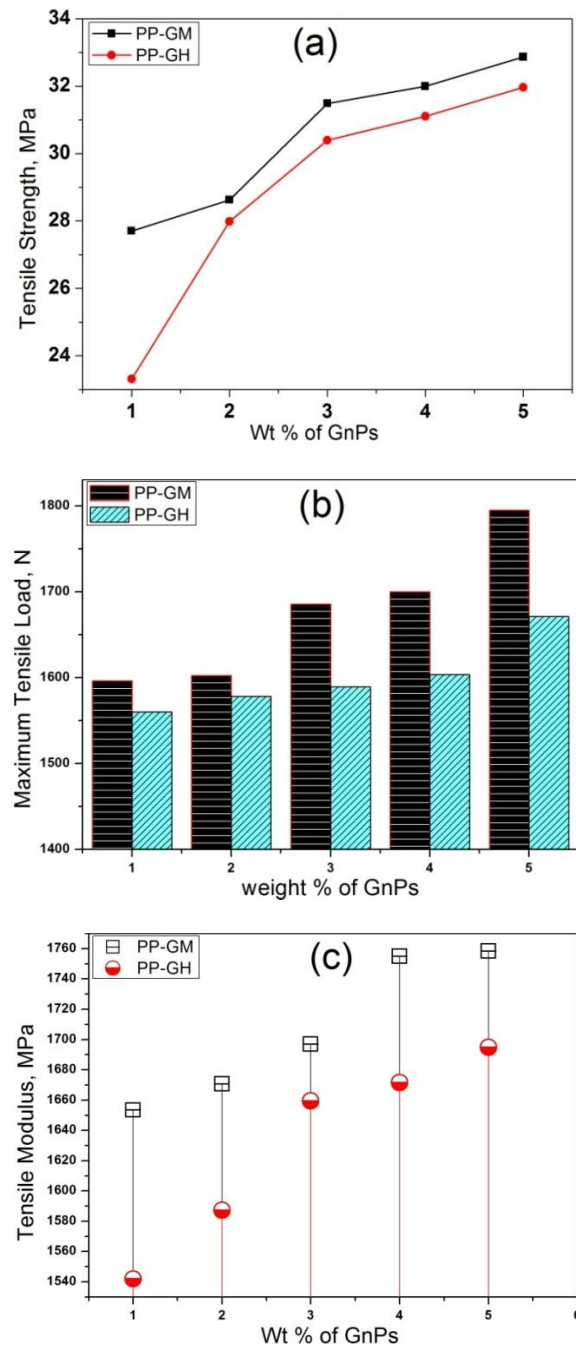


Figure 2. (a) Tensile strength, (b) maximum tensile load, and (c) tensile modulus of the polypropylene (PP)/GNP nanocomposites as a function of the GNP content.

Table 3. Extracted data pertaining to tensile properties.

Sample	Tensile Strength, MPa	Maximum Tensile Load, N	Tensile Modulus (E), MPa
PP	16.0 ± 1.5	1521.6 ± 25.1	1412.1 ± 40.0
PP-GH1	23.3 ± 0.3	1560.2 ± 26.1	1541.9 ± 40.8
PP-GH2	27.9 ± 0.4	1578.1 ± 27.2	1587.3 ± 41.2
PP-GH3	30.3 ± 1.8	1589.3 ± 27.8	1659.4 ± 43.5
PP-GH4	31.1 ± 1.3	1603.8 ± 30.2	1671.5 ± 43.8
PP-GH5	31.9 ± 1.5	1671.3 ± 31.1	1694.9 ± 44.0

Table 3. *Cont.*

Sample	Tensile Strength, MPa	Maximum Tensile Load, N	Tensile Modulus (E), MPa
PP-GM1	27.7 ± 0.9	1596.1 ± 25.1	1653.4 ± 41.3
PP-GM2	28.6 ± 0.7	1602.4 ± 28.3	1670.7 ± 40.3
PP-GM3	31.4 ± 0.3	1645.8 ± 32.1	1697.0 ± 42.5
PP-GM4	31.9 ± 1.8	1680.1 ± 32.8	1755.6 ± 41.3
PP-GM5	32.8 ± 2.1	1682.9 ± 32.9	1758.4 ± 40.1

This is due to the high modulus of the GNPs, which causes improvement in stress transfer at the filler and polymer matrix interface. A similar trend was also noticed for maximum tensile load carrying capacity and Young's modulus. The current outcomes are similar to the findings of several researchers [35,36]. The improved tensile properties are attributed to the increase in stiffness, which augments the adhesion between GNP particles and the PP matrix. The tensile strength increases from a minimum of 16 ± 1.5 MPa for virgin PP to approximately 33 ± 2.1 MPa for the PP-GM5 sample (more than 100% greater tensile strength). The GNP content alters the degree of dispersion and agglomeration and produces stiffer nanocomposites. Overall, the tensile strength, Young's modulus, and maximum tensile load carrying capacity improved as the GNP content increased. However, it is important to mention that the magnitudes of these properties were always higher for the nanocomposites carrying M25 grade GNPs. As the GNP sheet thickness decreases there will be improved interfacial bonding between PP and GNPs, causing a further reduction in agglomeration. This causes to achieve high degree of dispersion as compared to nanocomposites made from H25-grade GNPs. The decrease in sheet thickness increases the efficiency of reinforcement. A relevant study conducted by Fu et al [37] and Greer et al [38] considered the effect of size alone. They revealed that, the mechanical property is inversely proportional to the size of the filler. When Young's modulus is considered, a minimum value of ≈ 1413 MPa occurred for virgin PP. It increased up to ≈ 1695 MPa for the PP-GH5 composite, whereas a maximum value of ≈ 1759 MPa was reported for the PP-GM5 composite. The virgin PP carried a maximum tensile load of ≈ 1522 N and its capacity the increased to ≈ 1672 N and 1683 N for the PP-GH5 and PP-GM5 nanocomposites, respectively. The causes are obviously the increased surface areas that improved the efficiency of stress transfer between GNPs and the PP matrix. The high surface area for M25-grade GNPs increases the hindrance capacity for crack propagation, leading to an increase in strength [39]. The tensile stress–strain curves are shown in Figure 3. The virgin PP elongates up to 105% at breakage. Figure 3a,b show there is a significant decrease in elongation with increase in filler content. The % of elongation is 18% and is minimum for PP-GM5 nanocomposite, indicating it to be slightly ductile and tough composite. Reinforcing the M25-graded GNPs into the polymer matrix makes the composite more stiff as compared to filling the H2-graded GNPs, but on the other hand, decreases the stiffness to a great extent. This restricts the elongation and polymer chain movement.

The influence of the GNP content on flexural strength, flexural modulus, and maximum flexural load is shown in Figure 4 and the corresponding data are reported in Table 4. There was no significant improvement in flexural strength of PP with GNP loading. The neat PP showed a flexural strength of 50.7 MPa, which increased to 58.8 MPa when loaded with 5 wt% M25-grade GNPs. The flexural strength of PP-GM (PP-M25) nanocomposites was marginally higher than that of PP-H25 composites at all the loading rates, but as far as the flexural modulus is concerned, it increased to 1.6 times that of virgin PP. The stress–strain curves during the flexural tests are sketched in Figure 5. The causes of the improvement of flexural properties are attributed to the same mechanisms as previously discussed.

The influence of the GNP content on the impact strength is expressed in Figure 6, and the data are listed in the last column of Table 4. It is observed that there is a significant increase in impact strength with the GNP content, but it is to be noted that higher values are reported for H25-based polymer composites. The impact strength increased from 0.085 J for neat PP to 0.197 J (improved to 132%) for the PP-GH5 sample, but improvement up to 100% was seen for PP-GM5 composites. Loading thicker GNPs into the PP matrix caused graphene restacking by virtue of Van der Waals force of attraction within the particles and governing the impact strength. Graphene restacking for thicker GNPs decreased the energy dissipation during crack propagation, crack deflection and crack bridging [40,41].

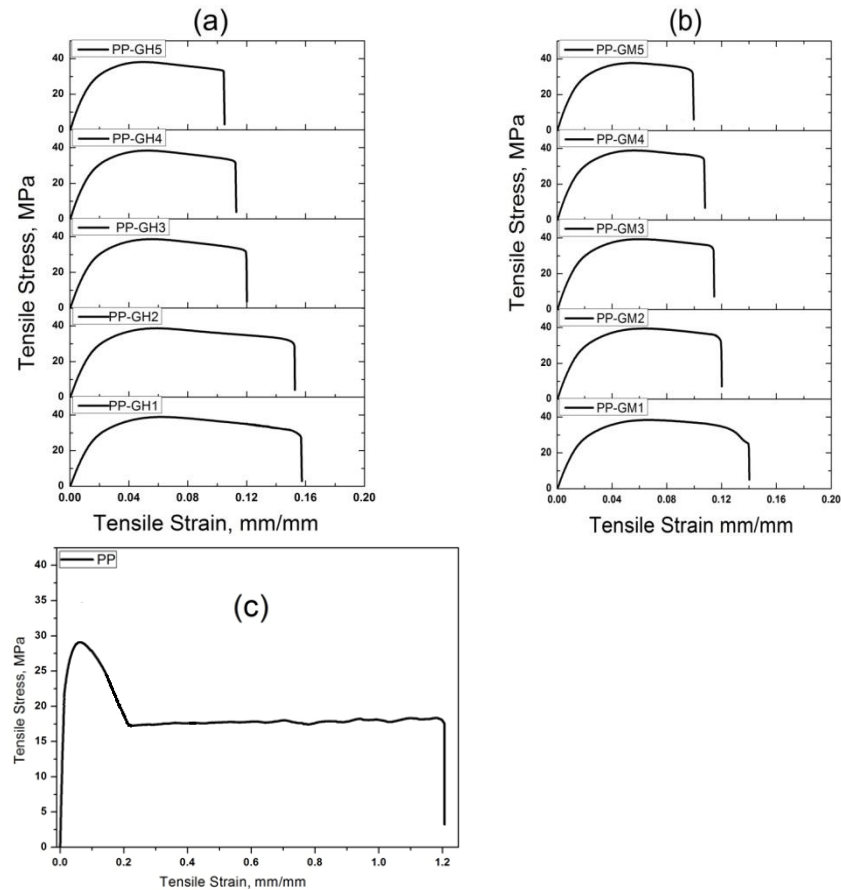


Figure 3. Tensile stress–strain diagrams of (a) PP-GH and (b) PP-GM composites as a function of increasing amount of GNPs; (c) Virgin PP.

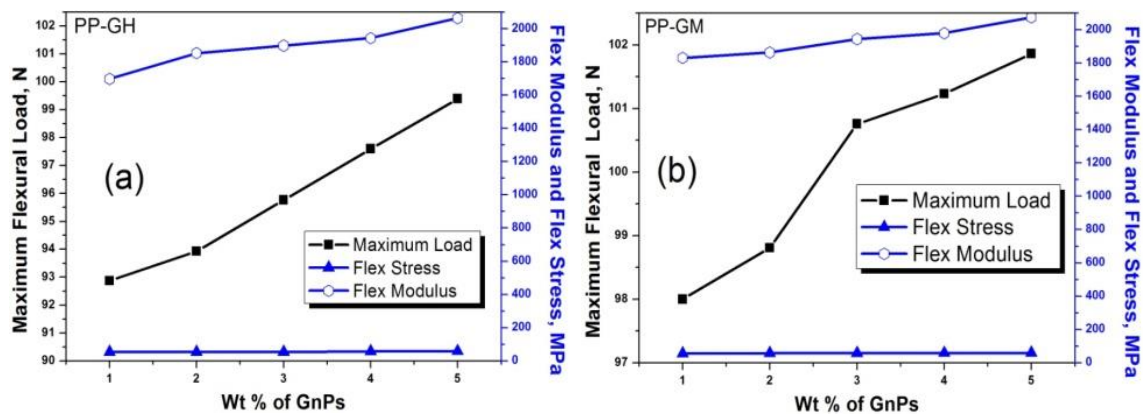


Figure 4. Flexural Strength, flexural modulus and maximum flexural load of (a) PP-GH and (b) PP-GM nanocomposites.

Table 4. Data sheet presenting the consequences of flexural and impact behaviour.

Sample.	Flexural Strength, MPa	Maximum Flexural Load, N	Flexural Modulus (E), MPa	Impact Strength, J
PP	50.7 ± 5.0	88.0 ± 11.2	1289.1 ± 245.1	0.085 ± 0.013
PP-GH1	52.8 ± 5.5	92.8 ± 11.7	1699.8 ± 246.8	0.129 ± 0.014
PP-GH2	53.7 ± 6.8	93.9 ± 11.2	1853.1 ± 246.9	0.154 ± 0.011
PP-GH3	53.9 ± 6.6	95.7 ± 11.9	1898.2 ± 247.3	0.187 ± 0.020
PP-GH4	57.2 ± 6.8	97.5 ± 12.3	1943.0 ± 247.4	0.195 ± 0.023
PP-GH5	58.3 ± 6.1	99.3 ± 12.2	2063.4 ± 249.5	0.197 ± 0.025
PP-GM1	56.2 ± 5.1	98.0 ± 10.6	1831.0 ± 250.1	0.112 ± 0.015
PP-GM2	56.9 ± 6.3	98.8 ± 10.9	1863.7 ± 250.3	0.128 ± 0.019
PP-GM3	57.7 ± 6.9	100.7 ± 11.3	1944.4 ± 256.9	0.133 ± 0.022
PP-GM4	58.5 ± 6.8	101.2 ± 12.2	1979.2 ± 257.3	0.164 ± 0.021
PP-GM5	58.8 ± 6.9	101.9 ± 12.3	2074.4 ± 258.8	0.174 ± 0.180

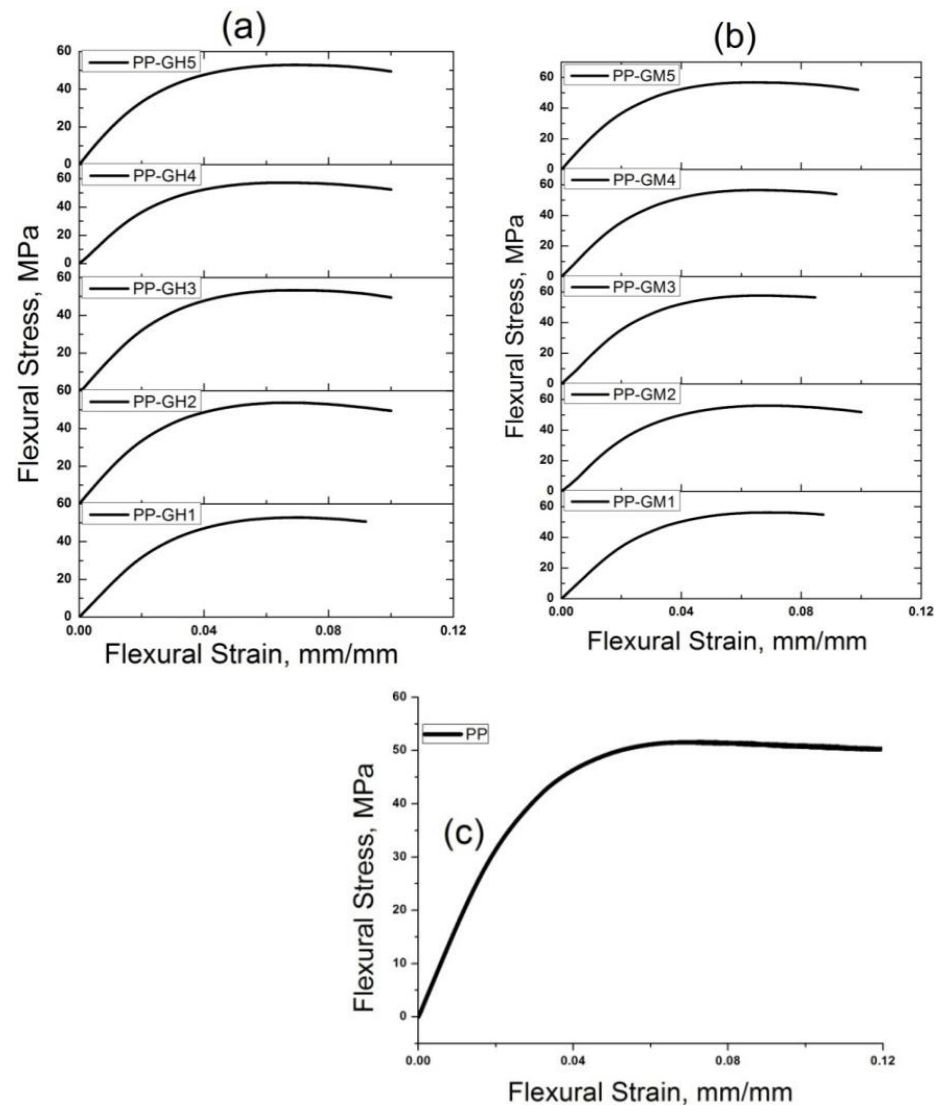


Figure 5. Flexural stress–strain curves of (a) PP-GH, (b) PP-GM nanocomposites, and (c) Virgin PP.

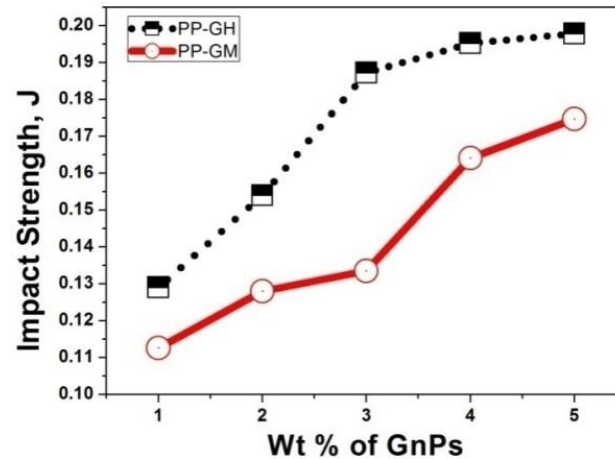


Figure 6. Variation of impact strength with GNP loading.

4.2. X-ray Diffraction and Microscopy

Figure 7 shows the XRD peaks for both neat PP and the prepared nanocomposites. The XRD of neat PP (Figure 7a) revealed the presence of α -form crystals. There were four peaks at 2θ values of 16.18, 19.32, 21.34, and 25.20. The PP peaks corresponded to (110), (040), (130), and (041) planes, respectively. No other crystal forms were observed for neat PP. The GNPs showed a single peak at $2\theta = 30.72$ and corresponded to the (002) plane due to the spacing between graphene units. As the GNPs were added, two new peaks appeared at 2θ angles of 24.28 and 29.43. These two peaks corresponded to the (111) and (060) planes of β -form crystals [42]. Therefore, the nanocomposites were dominated by the presence of α -form crystal peaks. In other words, reinforcing GNPs to PP boosts the crystallisation and helps to form different new crystals. The β crystals are formed for the nanocomposites with H25 and M25. Hence, it may be said that GNPs serve as nucleation sites in the polymer matrix [43,44], but strong β crystal peaks were observed for the polymer composite containing H25 at (111) plane.

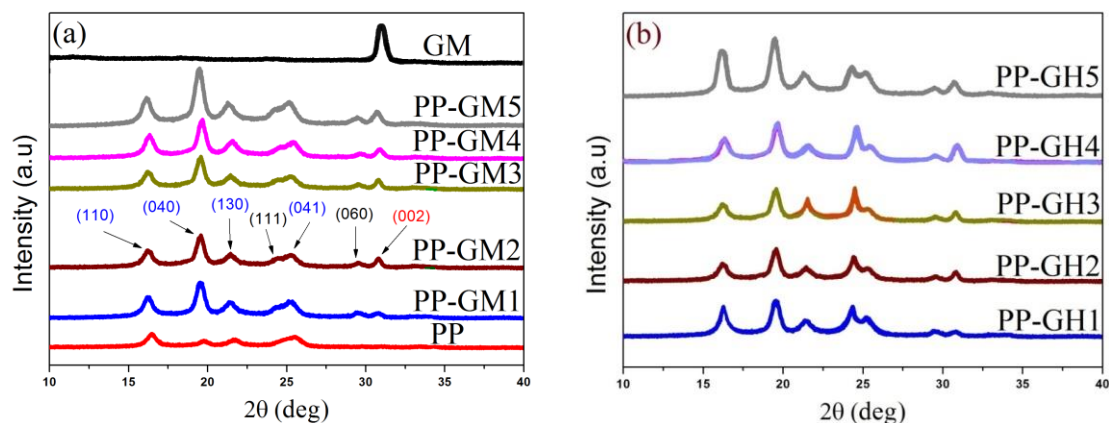


Figure 7. XRD curves of Virgin PP and PP nanocomposites reinforced with (a) M25 and (b) H25 respectively.

The increase in the sheet thickness decreased the saturation effect, causing random distribution of GNP particles in the matrix, so for same loading rates, thicker GNPs carry fewer particles per unit volume, and therefore the orientation space of the polymer chain with the GNPs decreases [45]. In Figure 8, the surface morphology of pure PP and PP/GNP nanocomposites characterised by FESEM is presented. A smooth and transparent surface is observed for neat PP (Figure 8a), with no other substances sticking to the surface. The surface of the GNP embedded nanocomposite is relatively tough. The surfaces of the nanocomposites reveal successful encapsulation of the nanoplatelets within the polymer

matrix. At a low filler level, there is less visibility of graphene nano sheets because of their low concentrations. As can be seen, at low concentrations there is satisfactory dispersion and the platelets uniformly stack throughout the matrix. Increasing the filler content makes the surface uneven and larger stacks emergence. This phenomenon restricts the polymer surface to accommodate the surplus GNP particles during melt mixing, so a greater fraction of the platelets cannot adhere to the polymer matrix and remain as large particles in the mixture. At high loading rates for H25-graded nanoplatelets there is delamination of sheets and hence large form. Phenomena such as bending and buckling do not exist for the composite with M25 platelets due its lower thickness. This boosts the reinforcement efficiency and dispersion and decreases agglomeration.

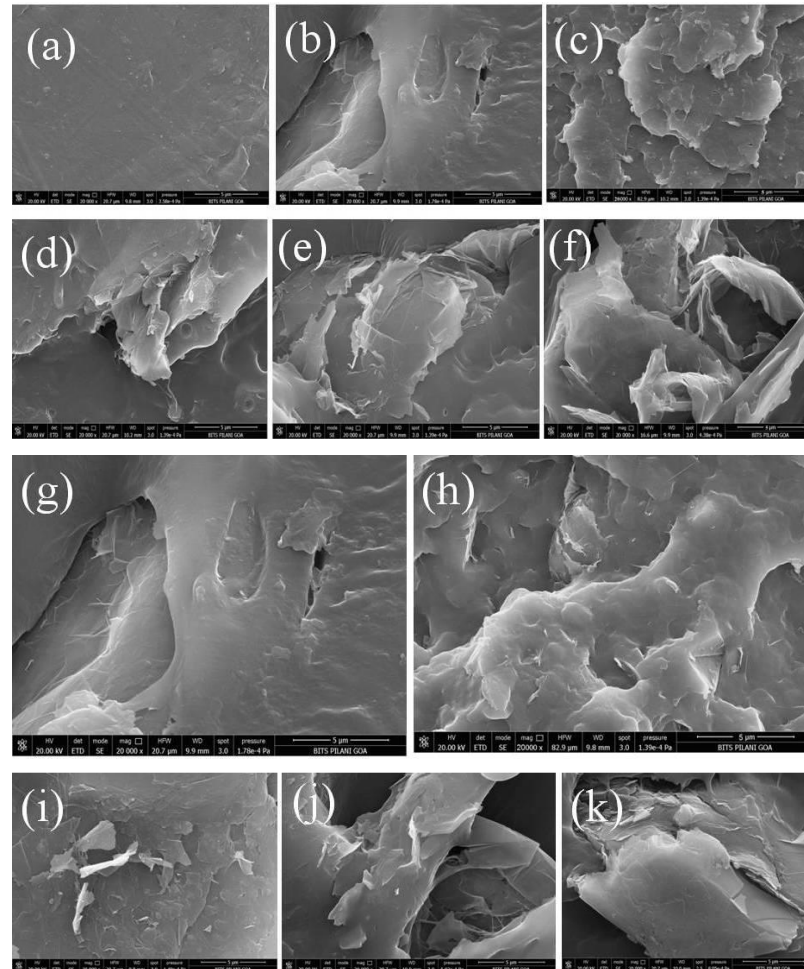


Figure 8. FESEM images of (a) neat PP, (b–f) PP-H25 and (g–k) PP-M25 nanocomposites with 1, 2, 3, 4 and 5 wt% GNPs respectively.

The crystallization behavior was further studied by PLM. As stated earlier, both the cooling and heating stages were used to facilitate the analysis. The spherulite morphologies are shown in Figure 9 for virgin PP and H25-loaded composites. The PLM study reveals the presence of GNP changed the crystallisation rate of virgin PP. Figure 9a reflects the spherulite structure of PP and no other crystal phases were seen. The GNP addition initiated the induction effect on the PP's β -phase crystal. This phenomenon is attributed to the possible nucleation between PP and GNP. The appearances of spherulites were clear in virgin PP, with large spherulite sizes. Adding GNP boosts nucleation and forms more nucleation sites and decreases crystal sizes [46–48]. From this study, it is evident that GNP acts as a successful nucleating agent in PP matrix. The results are in good agreement with XRD reports.

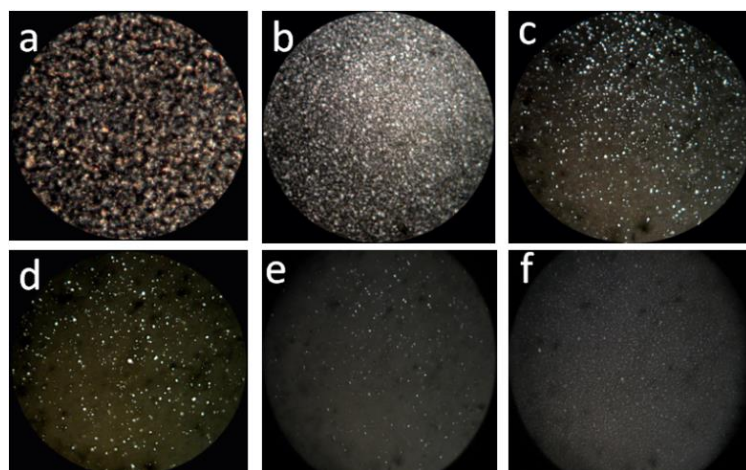


Figure 9. Spherulite morphology of (a) virgin PP, (b–f) PP-H25 nanocomposites containing 1, 2, 3, 4 and 5 wt% GNPs respectively at 130 °C and 10× magnification.

4.3. Crystallisation and Dynamic Mechanical Properties

DSC is a practical analysis tool for finding the melt and crystallization behaviour of polymeric materials. In this study both the melt (T_m) and crystallisation (T_c) temperatures were evaluated by using DSC as a function of the GNP content. The extracted results are reported in Table 5. An insight into the correlation between T_c and GNP concentration is illustrated in Figure 10. Addition of GNPs increased the crystallisation temperature due to its nucleating effects. As the sheet thickness decreased there was augmentation of nucleating effects. For 5 wt% GNP content, T_c increased by 4.8 °C for M25, whereas H25 increased T_c by 2.7 °C. This is because of better dispersion and increase in the surface area of M25. The thinner GNPs catalysed heterogeneous nucleation and hence facilitate crystallisation at higher temperatures. In this study, the T_c was largely influenced by the GNP content, whereas the degree of crystallisation (X_c) of the PP/GNP composites did not change much. The studied virgin PP has 60% X_c , which increased up to 62% for M25. The improvement in T_m by adding GNP was relatively low. This was due to an invariant α crystal form in polypropylene and signified that T_m is a function of the type of crystal form [49]. Thus, the crystal size of polypropylene had no influence on the T_m for higher GNP loading.

Table 5. Effect of GNP loading on the crystallization behavior of all the samples.

Sample	T_c , °C	T_m , °C	ΔT , °C	ΔH_c , J/g	ΔH_m , J/g	X_c , %
PP	123.4	162.6	39.2	171.5	124.8	60
PP-GH1	124.0	162.7	38.7	127.2	124.3	60
PP-GH2	124.4	162.9	38.5	125.4	124.1	60
PP-GH3	125.1	163.1	38.0	122.3	124.0	61
PP-GH4	125.3	163.2	37.9	119.0	123.9	61
PP-GH5	126.1	163.3	37.2	117.2	123.8	61
PP-GM1	127.0	162.8	35.8	130.3	123.7	60
PP-GM2	127.4	163.0	35.6	127.3	123.5	61
PP-GM3	127.6	163.2	35.6	124.6	123.4	61
PP-GM4	128.0	163.9	35.6	122.2	123.2	61
PP-GM5	128.2	164.0	35.8	119.0	123.1	62

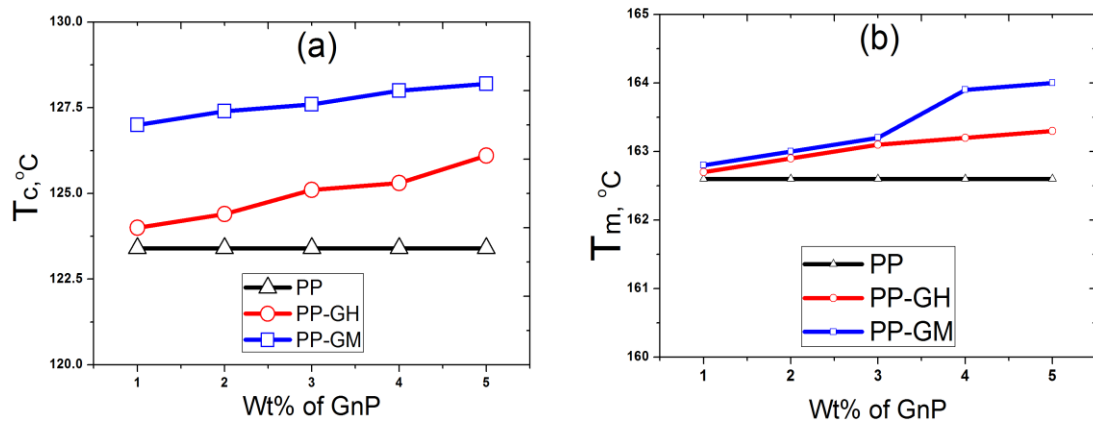


Figure 10. Variation of (a) crystallisation and (b) melt temperatures of the prepared nanocomposites with GNP content.

The effect of the GNP content on storage modulus and loss tangent ($\tan\delta$) of polypropylene was studied by conducting DMA. The experimental curves are shown in Figure 11. The tests were conducted starting from about 20 °C up to a temperature of 160 °C, which is very close to the melting temperature of PP. The literature reveals the glass transition temperature (T_g) to be in the range -20 to 0 °C [50]. Figure 11a,b shows an increase in storage modulus with GNP addition. As graphene is the stiffest material in nature, its reinforcement to PP increases the rigidity without changing the final processing temperature (because T_m does not change appreciably). The slope of the storage modulus curves almost constant up to 30 °C and represented the glassy state. There was a significant drop in storage modulus between 30 to about 90 °C (i.e., a sharp increase in $\tan\delta$). Within this temperature range, the nanocomposite behaviour is very similar to glass transition phase and may be called a relaxation phase or 2nd glass transition range, where the flow behaviour sharply changes. Regardless of GNP wt% the $\tan\delta$ value did not vary within 95–120 °C (Figure 11c) for H25 and reflected the rubbery plateau phase. Beyond 120 °C, the flow region exists, but for PP/M25 nanocomposites, the rubbery phase existed between 95 and 130 °C. For an insight into the storage modulus and loss tangent, the extracted data corresponding to 60 °C are reported in Table 6. Both the properties increased linearly with GNP loading as much as the tensile modulus. Comparing Figure 11a,b, it is seen that the storage modulus of the nanocomposites made from H25 and M25 changed identically with temperature. However, the M25 GNPs are thinner and have a higher interfacial surface area, which helps the effective arrangement inside the PP matrix. This leads to efficient stress transfer from the PP chain to the filler [51,52]. M25 GNPs satisfactorily boosted the stiffness. For an instant, reinforcing 5 wt% M25 and H25 GNP increased the storage modulus of PP by 54% and 30%, respectively. Nanocomposites filled with H25 are less stiff and assists to form aggregates and clusters. This phenomenon prevents stress distribution and causes a noteworthy reduction in properties.

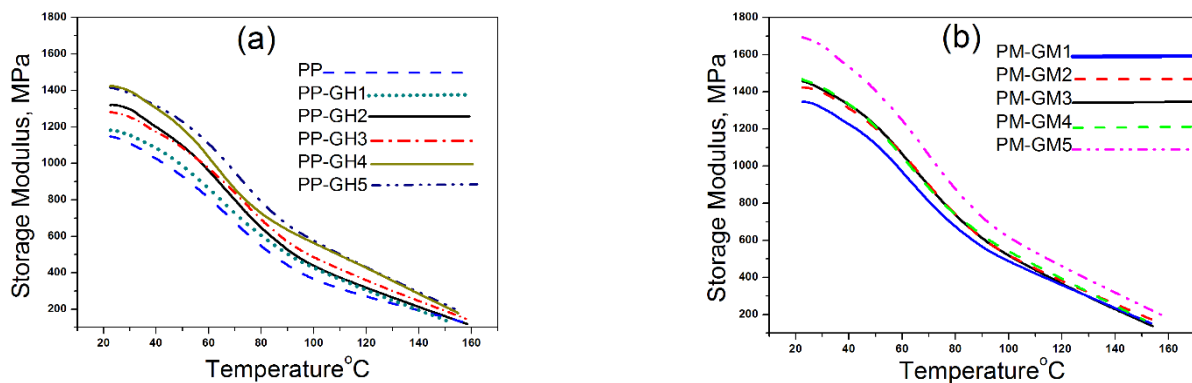


Figure 11. Cont.

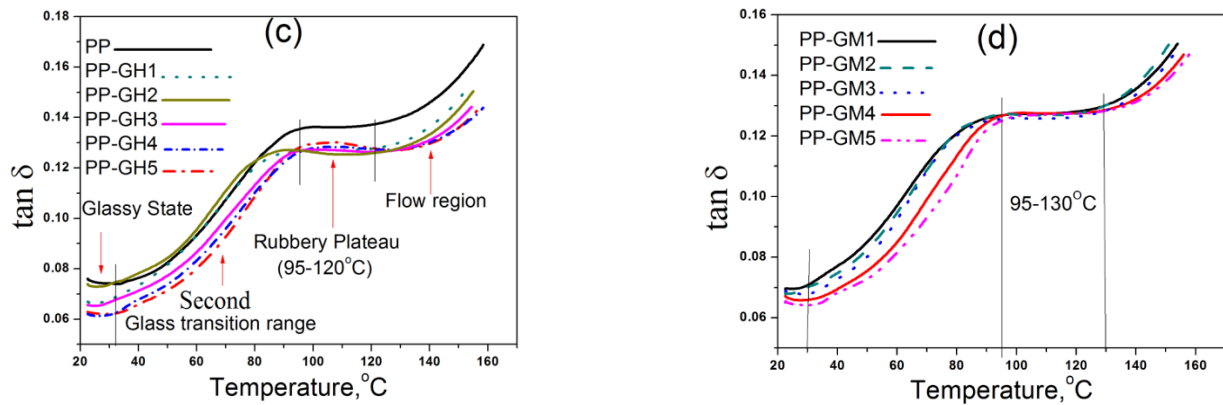


Figure 11. DMA curves of the prepared nanocomposites (a,b) storage modulus and (c,d) loss tangent.

Table 6. Data pertaining to DMA properties of the nanocomposites at 60 °C.

Sample	Storage Modulus, MPa	tanδ
PP	806.6	0.97420
PP-GH1	822.2	0.09598
PP-GH2	858.3	0.09504
PP-GH3	956.1	0.09360
PP-GH4	1046.9	0.09354
PP-GH5	1063.3	0.09277
PP-GM1	965.3	0.08689
PP-GM2	969.2	0.08528
PP-GM3	1029.2	0.08355
PP-GM4	1103.9	0.08182
PP-GM5	1242.1	0.08041

4.4. Thermal Stability of Nanocomposites

The thermal stability of the prepared PP/GNP composites was studied by carrying out TGA experiments. The resulting curves are shown in Figure 12. Some of the extracted parameters are tabulated in Table 7. The temperatures corresponding to beginning of degradation (TD) stage, 10% weight loss (T10), 50% weight loss (T50), and residual weight (TR) are reported in Table 7. The values of the as-mentioned parameters increased with the GNP content. The principal cause of improved thermal stability is due to formation of a mass transfer barrier, which obstructs the diffusion of degraded products to the polymer external surface [53,54]. GNP acts as barrier for the movement of the volatile gases formed during degradation from the inside of the composite to the polymer surface, so the volatile gases generated during decomposition are trapped within the composite and cannot escape. This is so called tortuous path effect, which delays degradation and char formation, improves the thermal stability. However, in this study, the M25 GNPs showed efficient thermal stability as compared to H25. It is noteworthy to discuss here that, the higher surface area of the thinner GNPs (M25) plays the key role in this context [55–57]. Several studies [58–61] have been conducted, showing the improvement of thermal stability by reinforcing GNP. The GNP particles restrict the mobility of the polymer chain, causing the increase in energy required for degradation and making the nanocomposite more thermally stable [62–66]. The thinner GNP sheet allows better dispersion inside the polymer matrix and improves thermal conduction. The advanced distribution of the thinner GNPs within the PP matrix boosts the thermal stability.

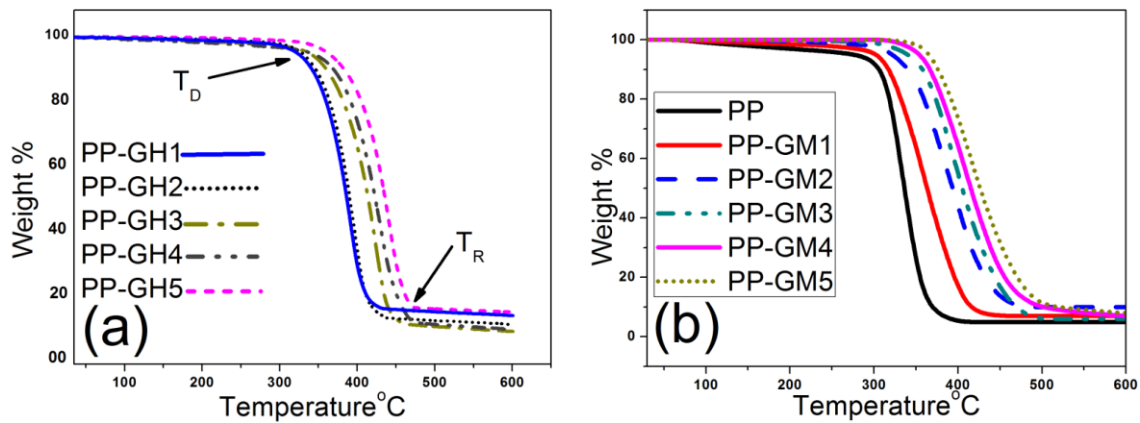


Figure 12. Thermogravimetric analysis (TGA) curves of PP composites incorporated with (a) H25 and (b) M25.

Table 7. TGA results of virgin PP and its composites reinforced with graphene nanoplatelets.

Sample	T _D , °C	T ₁₀ , °C	T ₅₀ , °C	T _R , °C
PP	301.5	307.3	336.2	400.3
PP-GH1	317.3	339.7	380.5	418.2
PP-GH2	320.2	346.7	392.6	434.3
PP-GH3	325.3	359.2	406.1	455.1
PP-GH4	344.6	368.6	417.8	474.3
PP-GH5	359.4	383.2	427.3	477.5
PP-GM1	320.9	343.2	386.2	423.8
PP-GM2	324.6	350.5	395.6	452.4
PP-GM3	332.5	360.6	415.5	484.9
PP-GM4	349.4	370.7	424.6	490.6
PP-GM5	372.3	387.4	437.5	503.1

5. Conclusions

The authors have successfully incorporated GNP into PP via melt mixing and injection moulding. The effects of the GNP content on different properties of PP are thoroughly studied. The performance of the PP/GNP composite has been investigated by various tests, viz. mechanical, thermal, etc. Reinforcing GNP to PP improves mechanical strength and thermal stability. Regardless of GNP type, at 5 wt% loading, the tensile strength improved by about 100%, the maximum tensile load carrying capacity improved up to ≈10%, the flexural strength increased more than 15%, and the impact strength increased more than 104%. The effect of sheet thickness was successfully evaluated. Thick graphene nanoplatelets make the composite heterogeneous and a stratifying material. Thicker platelet enhances the stacking of sheets, but thinner platelets are beneficial to improve tensile and flexural strength but reduce impact strengths. PP composites incorporated with thin GNPs exhibited better thermal stability based on evaluating TD, T10, T50, and TR. Thick GNPs transfer heat across the entire nanocomposite and boost the degradation. Adding GNP to PP exerts a nucleating effect and increases TC. However, XC, Tm was not significantly increased. The DMA test signified the simultaneous increase in storage modulus and loss tangent by adding GNP. Our study claims thinner GNPs facilitate overall dispersion and hinder efficient inter-particle contact. In conclusion, the sheet thickness of GNPs has a significant influence on the performance efficiency of the final composites, so thinner GNP sheets are recommended for all-around performance.

Author Contributions: Conceptualization, H.S. and B.M.; Methodology, H.S.; Software, B.M.; Validation, P.S., R.M. and D.S.; Formal Analysis, H.S.; Investigation, B.M.; Resources, D.S.; Data Curation, D.S.; Writing—Original Draft Preparation, H.S.; Writing—Review & Editing, H.S.; Visualization, R.M.; Supervision, P.S.; Project Administration, H.S.; Funding Acquisition, H.S., B.M., P.S., R.M. and D.S. All authors have read and agreed to the published version of the manuscript.

Funding: This research received no external funding.

Conflicts of Interest: The authors declare no conflict of interest.

References

1. Tjong, T.; Chin, S. Polymer composites with graphene nanofillers: Electrical properties and applications. *J. Nanosci. Nanotechnol.* **2014**, *14*, 1154–1168. [[CrossRef](#)] [[PubMed](#)]
2. Sengupta, R.; Bhattacharya, M.; Bandyopadhyay, S.; Bhowmick, A.K. A review on the mechanical and electrical properties of graphite and modified graphite reinforced polymer composites. *Prog. Polym. Sci.* **2011**, *36*, 638–670. [[CrossRef](#)]
3. Zhu, Y.; Murali, S.; Cai, W.; Li, X.; Suk, J.W.; Potts, J.R.; Ruoff, R.S. Graphene-based materials: Graphene and graphene oxide: Synthesis, properties, and applications. *Adv. Mater.* **2010**, *22*, 3903–3958.
4. Ma, P.C.; Siddiqui, N.A.; Marom, G.; Kim, J.K. Dispersion and functionalization of carbon nanotubes for polymer-based nanocomposites: A review. *Compos. Part A Appl. Sci. Manuf.* **2010**, *41*, 1345–1367. [[CrossRef](#)]
5. Papageorgiou, D.G.; Kinloch, I.A.; Young, R.J. Mechanical properties of graphene and graphene-based nanocomposites. *Prog. Mater. Sci.* **2017**, *90*, 75–127. [[CrossRef](#)]
6. Sahoo, N.G.; Rana, S.; Cho, J.W.; Li, L.; Chan, S.H. Polymer nanocomposites based on functionalized carbon nanotubes. *Prog. Polym. Sci.* **2010**, *35*, 837–867. [[CrossRef](#)]
7. Huang, C.; Cheng, Q. Learning from nacre: Constructing polymer nanocomposites. *Compos. Sci. Technol.* **2017**, *150*, 141–166. [[CrossRef](#)]
8. Huang, X.; Qi, X.; Boey, F.; Zhang, H. Graphene-based composites. *Chem. Soc. Rev.* **2012**, *41*, 666–686. [[CrossRef](#)]
9. Sutar, H.; Sahoo, P.C.; Sahu, P.S.; Sahoo, S.; Murmu, R.; Swain, S.; Mishra, S.C. Mechanical, thermal and crystallization properties of polypropylene (PP) reinforced composites with high density polyethylene (HDPE) as matrix. *Mater. Sci. Appl.* **2018**, *9*, 502–515. [[CrossRef](#)]
10. Sutar, H.; Maharana, H.S.; Dutta, C.; Murmu, R.; Patra, S. Strain rate effects on tensile properties of HDPE-PP composite prepared by extrusion and injection moulding method. *Mater. Sci. Appl.* **2019**, *10*, 205–215. [[CrossRef](#)]
11. Sahoo, P.C.; Murmu, R.; Patra, S.C.; Dutta, C.; Sutar, H. Electrical behaviour and spherulites morphology of HDPE/PP polyblends with HDPE as base material. *Mater. Sci. Appl.* **2018**, *9*, 837–843. [[CrossRef](#)]
12. Luo, G.; Li, W.; Liang, W.; Liu, G.; Ma, Y.; Niu, Y.; Li, G. Coupling effects of glass fiber treatment and matrix modification on the interfacial microstructures and the enhanced mechanical properties of glass fiber/polypropylene composites. *Compos. B Eng.* **2017**, *111*, 190–199. [[CrossRef](#)]
13. Nascimento, E.M.; Eiras, D.; Pessan, L.A. Effect of thermal treatment on impact resistance and mechanical properties of polypropylene/calcium carbonate nanocomposites. *Compos. B Eng.* **2017**, *91*, 228–234. [[CrossRef](#)]
14. Patti, A.; Russo, P.; Acierno, S. The effect of filler functionalization on dispersion and thermal conductivity of polypropylene/multi wall carbon nanotubes composites. *Compos. B Eng.* **2016**, *94*, 350–359. [[CrossRef](#)]
15. Gonzalez-Chi, P.I.; Rodríguez-Uicab, O.; Martín-Barrera, C.; Uribe-Calderon, J.; Canché-Escamilla, G.; Yazdani-Pedram, M.; Avilés, F. Influence of aramid fiber treatment and carbon nanotubes on the interfacial strength of polypropylene hierarchical composites. *Compos. B Eng.* **2017**, *122*, 16–22. [[CrossRef](#)]
16. Ahmad, S.R.; Young, R.J.; Kinloch, I.A. Raman spectra and mechanical properties of graphene/polypropylene nanocomposites. *Int. J. Chem. Eng. Appl.* **2015**, *6*, 1–5.
17. Yang, K.; Endoh, M.; Trojanowski, R.; Ramasamy, R.P.; Gentleman, M.M.; Butcher, T.A.; Rafailovich, M.H. The thermo-mechanical response of PP nanocomposites at high graphene loading. *Nanocomposites* **2015**, *1*, 126–137. [[CrossRef](#)]
18. Liang, J.-Z. Effects of tension rates and filler size on tensile properties of polypropylene/graphene nano-platelets composites. *Compos. B Eng.* **2019**, *167*, 241–249. [[CrossRef](#)]
19. El Achaby, M.; Arrakhiz, F.E.; Vaudreuil, S.; el Kacem Quiss, A.; Bousmina, M.; Fassi-Fehri, O. Mechanical, thermal, and rheological properties of graphene-based polypropylene nanocomposites prepared by melt mixing. *Polym. Compos.* **2012**, *33*, 733–744. [[CrossRef](#)]
20. Kuilla, T.; Bhadra, S.; Yao, D.; Kim, N.H.; Bose, S.; Lee, J.H. Recent advances in graphene-based polymer composites. *Prog. Polym. Sci.* **2010**, *35*, 1350–1375. [[CrossRef](#)]
21. Geng, Y.; Li, J.; Wang, S.J.; Kim, J.K. Amino functionalization of graphite nanoplatelet. *J. Nanosci. Nanotechnol.* **2008**, *8*, 6238–6246. [[CrossRef](#)] [[PubMed](#)]
22. Dassan, E.G.B.; Rahman, A.A.A.; Abidin, M.S.Z.; Akil, H.M. Carbon nanotube-reinforced polymer composite for electromagnetic interference application: A review. *Nanotechnol. Rev.* **2020**, *9*, 768–788. [[CrossRef](#)]
23. Kalaitzidou, K.; Fukushima, H.; Miyagawa, H.; Drzal, L.T. Flexural and tensile moduli of polypropylene nanocomposites and comparison of experimental data to Halpin-Tsai and Tandon-Weng models. *Polym. Eng. Sci.* **2007**, *47*, 1796–1803. [[CrossRef](#)]

24. Al-Saleh, M.A.; Yussuf, A.A.; Al-Enezi, S.; Kazemi, R.; Wahit, M.U.; Al-Shammari, T.; Al-Banna, A. Polypropylene/graphene nanocomposites: Effects of GNP loading and compatibilizers on the mechanical and thermal properties. *Materials* **2019**, *12*, 3924. [[CrossRef](#)] [[PubMed](#)]
25. Jun, Y.S.; Um, J.G.; Jiang, G.; Lui, G.; Yu, A. Ultra-large sized graphene nano-platelets (GnPs) incorporated polypropylene (PP)/GnPs composites engineered by melt compounding and its thermal, mechanical, and electrical properties. *Compos. B Eng.* **2018**, *133*, 218–225. [[CrossRef](#)]
26. Liang, J.Z.; Du, Q.; Tsui, G.C.; Tang, C.Y. Tensile properties of graphene nano-platelets reinforced polypropylene composites. *Compos. B Eng.* **2016**, *95*, 166–171. [[CrossRef](#)]
27. Chunhui, S.; Mu, P.; Runzhang, Y. The effect of particle size gradation of conductive fillers on the conductivity and the flexural strength of composite bipolar plate. *Int. J. Hydrogen Energy* **2008**, *33*, 1035–1039. [[CrossRef](#)]
28. Bafana, A.P.; Yan, X.; Wei, X.; Patel, M.; Guo, Z.; Wei, S.; Wujcik, E.K. Polypropylene nanocomposites reinforced with low weight percent graphene nanoplatelets. *Compos. B Eng.* **2017**, *109*, 101–107. [[CrossRef](#)]
29. Pedrazzoli, D.; Pegoretti, A.; Kalaitzidou, K. Understanding the effect of silica nanoparticles and exfoliated graphite nanoplatelets on the crystallization behavior of isotactic polypropylene. *Polym. Eng. Sci.* **2015**, *55*, 672–680. [[CrossRef](#)]
30. Jun, Y.S.; Um, J.G.; Jiang, G.; Yu, A. A study on the effects of graphene nano-platelets (GnPs) sheet sizes from a few to hundred microns on the thermal, mechanical, and electrical properties of polypropylene (PP)/GnPs composites. *eXPRESS Polym. Lett.* **2018**, *12*, 885–897. [[CrossRef](#)]
31. Ajorloo, M.; Fasihi, M.; Ohshima, M.; Taki, K. How are the thermal properties of polypropylene/graphene nanoplatelet composites affected by polymer chain configuration and size of nanofiller? *Mater. Des.* **2019**, *181*, 108068. [[CrossRef](#)]
32. Wang, Q.; Wang, Y.; Meng, Q.; Wang, T.; Guo, W.; Wu, G.; You, L. Preparation of high antistatic HDPE/polyaniline encapsulated graphene nanoplatelet composites by solution blending. *RSC Adv.* **2017**, *7*, 2796–2803. [[CrossRef](#)]
33. Mistretta, M.C.; Botta, L.; Vinci, A.D.; Ceraulo, M.; La Mantia, F.P. Photo-oxidation of polypropylene/graphene nanoplatelets composites. *Polym. Degrad. Stab.* **2019**, *160*, 35–43. [[CrossRef](#)]
34. Blaine, R.L. Thermal Applications Note. Polymer Heats of Fusion. 2002. Available online: <http://www.tainstruments.com/pdf/literature/TN048.pdf> (accessed on 11 January 2021).
35. An, J.E.; Jeon, G.W.; Jeong, Y.G. Preparation and properties of polypropylene nanocomposites reinforced with exfoliated graphene. *Fiber Polym.* **2012**, *13*, 507–514. [[CrossRef](#)]
36. Kim, M.S.; Yan, J.; Kang, K.-M.; Joo, K.H.; Kang, Y.J.; Ahn, S.H. Soundproofing ability and mechanical properties of polypropylene/exfoliated graphite nanoplatelet/carbon nanotube (PP/xGNP/CNT) composite. *Int. J. Precis. Eng. Manuf.* **2013**, *1*, 1087–1092. [[CrossRef](#)]
37. Fu, S.Y.; Feng, X.Q.; Lauke, B.; Mai, Y.W. Effects of particle size, particle/matrix interface adhesion and particle loading on mechanical properties of particulate–polymer composites. *Compos. B Eng.* **2008**, *39*, 933–961. [[CrossRef](#)]
38. Greer, J.R.; Oliver, W.C.; Nix, W.D. Size dependence of mechanical properties of gold at the micron scale in the absence of strain gradients. *Acta Mater.* **2005**, *53*, 1821–1830. [[CrossRef](#)]
39. Kalaitzidou, K.; Fukushima, H.; Drzal, L.T. Mechanical properties and morphological characterization of exfoliated graphite–polypropylene nanocomposites. *Compos. Part A Appl. Sci. Manuf.* **2007**, *38*, 1675–1682. [[CrossRef](#)]
40. Thomason, J.L.; Vlug, M.A. Influence of fibre length and concentration on the properties of glass fibre-reinforced polypropylene: 4. Impact properties. *Compos. Part A Appl. Sci. Manuf.* **1997**, *28*, 277–288. [[CrossRef](#)]
41. Rahman, N.A.; Hassan, A.; Yahya, R.; Lafia-Araga, R.A.; Hornsby, P.R. Micro-structural, thermal, and mechanical properties of injection-molded glass fiber/nanoclay/polypropylene composites. *J. Reinf. Plast. Compos.* **2012**, *31*, 269–281. [[CrossRef](#)]
42. Kalaitzidou, K.; Fukushima, H.; Askeland, P.; Drzal, L.T. The nucleating effect of exfoliated graphite nanoplatelets and their influence on the crystal structure and electrical conductivity of polypropylene nanocomposites. *J. Mater. Sci.* **2008**, *43*, 2895–2907. [[CrossRef](#)]
43. Kołodziej, A.; Długoń, E.; Świątek, M.; Ziabka, M.; Dawiec, E.; Gubernat, M.; Michalec, M.; Weselucha-Birczyńska, A. A Raman Spectroscopic Analysis of Polymer Membranes with Graphene Oxide and Reduced Graphene Oxide. *J. Compos. Sci.* **2021**, *5*, 20. [[CrossRef](#)]
44. Wu, H.; Rook, B.; Drzal, L.T. Dispersion optimization of exfoliated graphene nanoplatelet in polyetherimide nanocomposites: Extrusion, precoating, and solid state ball milling. *Polym. Compos.* **2013**, *34*, 426–432. [[CrossRef](#)]
45. Kalaitzidou, K. Exfoliated Graphite Nanoplatelets as Nanoreinforcement for Multifunctional Polypropylene Nanocomposites. Ph.D. Thesis, Michigan State University, East Lansing, MI, USA, 2006.
46. Cui, L.; Wang, P.; Zhang, Y.; Zhang, L.; Chen, Y.; Wang, L.; Guo, X. Combined effect of α -nucleating agents and glass fiber reinforcement on a polypropylene composite: A balanced approach. *RSC Adv.* **2017**, *7*, 42783–42791. [[CrossRef](#)]
47. Cui, L.; Wang, P.; Zhang, Y.; Zhou, X.; Xu, L.; Zhang, L.; Guo, X. Glass fiber reinforced and β -nucleating agents regulated polypropylene: A complementary approach and a case study. *J. Appl. Polym. Sci.* **2018**, *135*, 45768. [[CrossRef](#)]
48. Liu, Z.; Hao, B.; Zhang, Y. Control interfacial properties and tensile strength of glass fibre/PP composites by grafting poly (ethylene glycol) chains on glass fibre surface. *RSC Adv.* **2015**, *5*, 40668–40677. [[CrossRef](#)]
49. Xiao, W.; Wu, P.; Feng, J. Effect of β -nucleating agents on crystallization and melting behavior of isotactic polypropylene. *J. Appl. Polym. Sci.* **2008**, *108*, 3370–3379. [[CrossRef](#)]

50. Rahman, N.A.; Hassan, A.; Yahya, R.; Lafia-Araga, R.; Hornsby, P. Polypropylene/glass fiber/nanoclay hybrid composites: Morphological, thermal, dynamic mechanical and impact behaviors. *J. Reinf. Plast. Compos.* **2012**, *31*, 1247–1257. [[CrossRef](#)]
51. Prolongo, S.G.; Jiménez-Suárez, A.; Moriche, R.; Ureña, A. Graphene nanoplatelets thickness and lateral size influence on the morphology and behavior of epoxy composites. *Eur. Polym. J.* **2014**, *53*, 292–301. [[CrossRef](#)]
52. Mayoral, B.; Harkin-Jones, E.; Khanam, P.N.; AlMaadeed, M.A.; Ouederni, M.; Hamilton, A.R.; Sun, D. Melt processing and characterisation of polyamide 6/graphene nanoplatelet composites. *RSC Adv.* **2015**, *5*, 52395–52409. [[CrossRef](#)]
53. Zhao, S.; Chen, F.; Huang, Y.; Dong, J.-Y.; Han, C.C. Crystallization behaviors in the isotactic polypropylene/graphene composites. *Polymer* **2014**, *55*, 4125–4135. [[CrossRef](#)]
54. Gu, J.; Du, J.; Dang, J.; Geng, W.; Hu, S.; Zhang, Q. Thermal conductivities, mechanical and thermal properties of graphite nanoplatelets/polyphenylene sulfide composites. *RSC Adv.* **2014**, *4*, 22101–22105. [[CrossRef](#)]
55. Laachachi, A.; Burger, N.; Apaydin, K.; Sonnier, R.; Ferriol, M. Is expanded graphite acting as flame retardant in epoxy resin? *Polym. Degrad. Stab.* **2015**, *117*, 22–29. [[CrossRef](#)]
56. Um, J.G.; Jun, Y.-S.; Alhumade, H.; Krithivasan, H.; Lui, G.; Yu, A. Investigation of the size effect of graphene nano-platelets (GnPs) on the anti-corrosion performance of polyurethane/GnP composites. *RSC Adv.* **2018**, *8*, 17091–17100. [[CrossRef](#)]
57. Saleem, A.; Zhang, Y.; Gong, H.; Majeed, M.K.; Jing, J.; Lin, X.; Ashfaq, M.Z. Enhanced thermal conductivity and mechanical properties of a GNP reinforced Si₃N₄ composite. *RSC Adv.* **2019**, *9*, 39986–39992. [[CrossRef](#)]
58. Salavagione, H.J.; Gómez, M.A.; Martínez, G. Polymeric modification of graphene through esterification of graphite oxide and poly (vinyl alcohol). *Macromolecules* **2009**, *42*, 6331–6334. [[CrossRef](#)]
59. Verdejo, R.; Barroso-Bujans, F.; Rodriguez-Perez, M.A.; Antonio de Saja, J.; Lopez-Manchado, M.A. Functionalized graphene sheet filled silicone foam nanocomposites. *J. Mater. Chem.* **2008**, *18*, 2221. [[CrossRef](#)]
60. Mahmood, H.; Unterberger, S.H.; Pegoretti, A. Tuning Electrical and Thermal Properties in Epoxy/Glass Composites by Graphene-Based Interphase. *J. Compos. Sci.* **2017**, *1*, 12. [[CrossRef](#)]
61. Azizi, S.; Azizi, M.; Sabetzadeh, M. The Role of Multiwalled Carbon Nanotubes in the Mechanical, Thermal, Rheological, and Electrical Properties of PP/PLA/MWCNTs Nanocomposites. *J. Compos. Sci.* **2019**, *3*, 64. [[CrossRef](#)]
62. Behdinin, K.; Dastjerdi, R.M.; Safaei, B.; Qin, Z.; Chu, F.; Hui, D. Graphene and CNT impact on heat transfer response of nanocomposite cylinders. *Nanotechnol. Rev.* **2020**, *9*, 41–52. [[CrossRef](#)]
63. Parameswaranpillai, J.; Joseph, G.; Shinu, K.P.; Jose, S.; Salim, N.V.; Hameed, N. Development of hybrid composites for automotive applications: Effect of addition of SEBS on the morphology, mechanical, viscoelastic, crystallization and thermal degradation properties of PP/PS-xGnP composites. *RSC Adv.* **2015**, *5*, 25634–25641. [[CrossRef](#)]
64. Sultana, T.; Sultana, S.; Nur, H.P.; Khan, M.W. Studies on Mechanical, Thermal and Morphological Properties of Betel Nut Husk Nano Cellulose Reinforced Biodegradable Polymer Composites. *J. Compos. Sci.* **2020**, *4*, 83. [[CrossRef](#)]
65. Martin, I.; Saenz del Castillo, D.; Fernandez, A.; Güemes, A. Advanced Thermoplastic Composite Manufacturing by In-Situ Consolidation: A Review. *J. Compos. Sci.* **2020**, *4*, 149. [[CrossRef](#)]
66. Zhang, H.; Zhang, X.; Fang, Z.; Huang, Y.; Xu, H.; Liu, Y.; Wu, D.; Zhuang, J.; Sun, J. Recent Advances in Preparation, Mechanisms, and Applications of Thermally Conductive Polymer Composites: A Review. *J. Compos. Sci.* **2020**, *4*, 180. [[CrossRef](#)]